A&A 429, 543–557 (2005)
DOI: 10.1051/0004-6361:20041409

Astronomy & Astrophysics

Probing the embedded YSOs of the R CrA region through VLT-ISAAC spectroscopy⋆,⋆⋆

B. Nisini[1], S. Antoniucci[1,2], T. Giannini[1], and D. Lorenzetti[1]

[1] INAF-Osservatorio Astronomico di Roma, via di Frascati 33, 00040 Monteporzio Catone, Italy
e-mail: nisini@mporzio.astro.it
[2] Università degli Studi "Tor Vergata", via della Ricerca Scientifica 1, 00133 Roma, Italy

Received 4 June 2004 / Accepted 25 August 2004

Abstract. Near IR spectra at low ($R \sim 800$) and medium ($R \sim 9000$) resolution, obtained with ISAAC at VLT, have been used to pose constraints on the evolutionary state and accretion properties of a sample of five embedded YSOs located in the R CrA core. This sample includes three Class I sources (HH100 IR, IRS2 and IRS5), and two sources with NIR excesses (IRS6 and IRS3). IRS5 and IRS6 have been discovered to be binaries with a separation between the two components of 78 and 97 AU, respectively. Absorption lines, typical of late-type photospheres, have been detected in the medium resolution spectra of all the observed targets, including HH100 IR and IRS2 which have high values of infrared continuum veiling ($r_K = 6$ and 3, respectively). These two sources also present low resolution spectra rich in emission lines (HI, CO and plenty of other permitted lines from neutral atoms) likely originating in the disk-star-wind connected regions. Among the features observed in HH100 IR and IRS2, Na I at 2.205 μm and CO at 2.3 μm, which are more commonly used for stellar classification, are detected in emission instead of absorption. Several strong photospheric lines which lie around 2.12 and 2.23 μm and whose ratio is sensitive to both effective temperature and gravity are proposed as independent diagnostic tools for this type of sources. We derived spectral types, veiling and stellar luminosity for the five observed sources, which in turn have been used to infer their mass (ranging between 0.3–1.2 $M_\odot$) and age (between 10^5 and 10^6 yr) adopting pre-main sequence evolutionary tracks. We find that in HH100 IR and IRS2 most of the bolometric luminosity is due to accretion ($L_{\rm acc}/L_{\rm bol} \sim 0.8$ and 0.6 respectively), while the other three investigated sources, including the Class I object IRS5a, present low accretion activity ($L_{\rm acc}/L_{\rm bol} < 0.2$). Mass accretion rates of the order of 2×10^{-6} and 3×10^{-7} $M_\odot$ yr^{-1} are derived for HH100 IR and IRS2, respectively, i.e. higher by an order of magnitude than the average values derived for T Tauri stars. We observe a general correlation between the accretion luminosity, the IR veiling and the emission line activity of the sources. In particular, we find that the correlation between $L_{\rm acc}$ and $L_{\rm Br\gamma}$, previously reported for optical T Tauri stars, can be extended to the embedded sources, up to at least one order of magnitude larger line luminosity. A correlation between the accretion activity and the spectral energy distribution slope is recognizable with the notable exception of IRS5a. Our analysis therefore shows how the definition of the evolutionary stage of deeply embedded YSOs by means of IR colors needs to be refined.

Key words. stars: formation – infrared: stars – stars: individual: R CrA – line: formation

1. Introduction

During the first evolutionary stages of a young star the protostellar system is characterized by a variety of phenomena occurring in different regions of the circumstellar environment. These include the accretion disk, the magnetospheric accretion region, collimated jets and, in more embedded sources, the still not dispersed dusty envelopes. In T Tauri systems, where the contribution from the dusty envelope has become negligible, there is the possibility to disentangle, through observations at different wavelengths, the emission from the star itself from that of the different active circumstellar regions, and to define in detail the properties of the latter. Hence the stellar parameters of T Tauri stars have been derived through the observations of their optical and IR photospheric features (e.g. Luhman & Rieke 1998), their accretion regions revealed through the observation of the UV excesses over the stellar photosphere (e.g. Gullbring et al. 1998), and finally their collimated jets probed down to close to their base through high resolution observations of optical forbidden lines (e.g. Bacciotti et al. 2000). The possibility to separate the different emission components contributing to the stellar system has greatly advanced the comparison of observations with models describing the accretion and ejection mechanisms in these stars, as well as the disk evolution and dispersal. It is however of fundamental importance to understand how and if these models

⋆ Based on observations collected at the European Southern Observatory, Chile (ESO N.069.C-0269, 070.C.-0138, 063.I-0691).
⋆⋆ Appendix A is only available in electronic form at http://www.edpsciences.org

works for less evolved systems, where the circumstellar activity is much higher and the accretion luminosity is expected to dominate over the luminosity of the still forming star. To this aim, a sample of interesting objects to be investigated comprises sources with no optical counterpart, characterized by steeply rising IR Spectral Energy Distributions (SEDs) and with infrared colors indicating the presence of intrinsic excesses due to circumstellar dust (the so-called Class I sources). The standard paradigm is that most of these sources are protostars still embedded in their original infalling envelope and expected to derive most of their luminosity from accretion through a massive circumstellar disk. For such more embedded sources, however, the large extinction coupled with strong emission excesses due to the circumstellar envelope make the investigation of phenomena occurring very close to the protostar extremely difficult and thus their real nature remains often obscure. Infrared spectroscopy can significantly improve the study of the close environments of these sources, since different gas features which are present in the near IR atmospheric windows can be related to different emitting regions. The near IR spectra of these objects are often characterized by the presence of ionized (e.g. Fe^+), neutral (e.g. HI, He) and molecular (CO, H_2) emission lines. Such lines originate in the inner and warm regions of the disk, in the accretion region connecting the disk to the star, and in the related winds and jets, and consequently they have been used to probe such different environments (e.g. Nisini et al. 2002; Najita et al. 1996; Davis et al. 2002; Muzerolle et al. 1998). The large values of the IR excess characteristic of these source, however, produce a large veiling which makes it extremely difficult to infer their stellar properties by means of their underlying photospheric features and therefore to correlate the spectral probes of circumstellar activity with the physical parameters of the star itself.

Recently, the first direct observation of absorption lines from the photosphere of a Class I source in the ρ Oph cloud has been reported by Greene & Lada (2002). The observed features are typical of late type stars, confirming the low mass nature of these sources, and have been used to determine for the first time the stellar properties of one of such highly obscured object, which was found to have ~70% of its luminosity due to accretion. The potential of high-resolution near IR spectroscopy to reveal the central protostellar source characteristics opens in turn the possibility to both derive the masses and ages of these young objects and infer quantitatively the mass accretion rate and accretion luminosity to be compared with those of expected more evolved sources. In order to make this comparison significant it is also important to have this information for a sample as large as possible of embedded sources, such as to better constrain their global accretion properties. In this paper we report the results of an analysis of medium/high resolution near IR spectra of a sample of embedded young stellar objects of the nearby R CrA star forming cloud (D = 130 pc, Marraco & Rydgren 1981). The selection of sources from the same cloud ensures that the properties of the sources reflect intrinsic differences and not the different characteristics of the hosting cloud. The aim of this paper is twofold: 1) to infer, through the observations of photospheric features, the stellar physical parameters of the considered objects and from these indirectly derive their ages, accretion luminosities and mass accretion rates. This information will be used to understand to which extent the spectral energy distribution of embedded IR sources is really indicative of their evolutionary stage; 2) to establish if there is a correlation between the accretion luminosity of the embedded stars and the occurrence and luminosity of their IR emission lines in order to have an indirect instrument to quantitatively derive the accretion rate from simple observational tools. We describe the considered sample in Sect. 2 and the observations obtained at VLT with the ISAAC instrument in Sect. 3. In Sects. 4 and 5 the characteristics of the emission line spectra are described, while in Sects. 6 and 7 we present the procedure adopted to derive the stellar and circumstellar properties from the detected absorption features. Finally, in Sect. 8 we discuss the implications of our findings.

2. Description of the selected sample

The sources investigated in this paper have been taken from the sample of IR young stellar objects in the R CrA cloud core listed by Wilking et al. (1997). From this list we have selected all the IR sources with K magnitudes smaller than 10.5 mag and IR colors compatible with the locus of young embedded protostars with intrinsic IR excesses (Lada & Adams 1992). The list of sources is presented in Table 1 with their coordinates, IR magnitudes and luminosities, when available. All the sources have luminosities ranging between 1 and 15 $L_\odot$, thus they are expected to be low mass young stellar objects.

Three of the considered sources, namely HH100 IR, IRS2 and IRS5, can be classified as Class I protostars on the basis of their spectral energy distributions (having spectral index between 2 and 10 μm > 0, Wilking et al. 1986). These three sources are known to have large dusty envelopes as testified by the presence of strong ice bands and silicate features in their 3, 5 and 10 μm spectra (Brooke et al. 1999; Whittet et al. 1996; Alexander et al. 2003; Chen & Graham 1993; Pontoppidan et al. 2003). HH100 IR has also been suggested as the driving source of the Herbig Haro objects HH101 and HH99 (Hartigan & Graham 1987) and of a bipolar molecular outflow (Anglada et al. 1989).

3. Observations

Observations were carried out at VLT/UT1 with the ISAAC spectrograph in SW mode on 12 and 13 July, 2002. At the spatial resolution provided by ISAAC (i.e. 0.14 arcsec/pixel), the sources IRS5 and IRS6 were recognized to be binaries, with a separation of ~0.6 and 0.75 arcsec (i.e. 78 and 97 AU), respectively. Figure 1 shows H and K images obtained from VLT pre-imaging of these stars, in which the two components that we named a and b are clearly visible. Owing to their alignment in the sky, a single slit, with a position angle of 32.6°, was adopted to observe simultaneously IRS5a and b, and IRS6a.

Low resolution spectra through the J (1.1−1.4 μm), SH (1.4−1.82 μm) and SK (1.82−2.5 μm) filters were acquired with a slit aperture of 0.″6 corresponding to a resolution ranging from 750 (in the K band) to 960 (in the J band). For each source

Table 1. Observed sample.

Source	α (2000)	δ (2000)	K	$(K-L)$	$(H-K)$	$(J-H)$	α^a	Ref.^{b}	$L_{\rm bol}$
			magnitudes						($L_\odot$)
IRS2 (TS13.1)	19 01 41.5	−36 58 29	7.16	2.72	2.73	4.07	0.98	TS	12^c
			7.2	–	2.7	3.9		SOFI	
IRS5 (TS2.4)	19 01 48.0	−36 57 19	10.33	2.75	3.32	3.89	1.12	TS	3^c
IRS5a			10.9	–	3.8	–		ISAAC	2
IRS5b			11.5	–	3.4	–		ISAAC	
IRS6 (TS2.3)	19 01 50.6	−36 56 38	10.34	1.74	2.37	3.64	∼0	TS	∼0.6^d
IRS6a			11.1	–	2.2	–		ISAAC	∼0.3
IRS6b			11.7	–	3.1	–		ISAAC	
HH100 IR (TS2.6)	19 01 50.7	−36 58 10	8.04	3.36	3.5	4.87	1.47	TS	14^c
			7.4	–	2.5	4.1		SOFI	
IRS3 (TS4.4)	19 02 05.1	−36 58 56	8.64	–	2.02	2.26		TS	∼0.3^d
			9.50	–	0.93	0.14		B92	

[a]Spectral index (d log(λF_λ)/d log λ) between 2 and 10 μm.
[b]Origin of photometric data: TS = Taylor & Storey (1984), SOFI = our NTT-SOFI observations (March 2003), ISAAC = VLT-ISAAC archive data (April 1999), B92 = Burton et al. (1992).
[c]From Wilking et al. (1992).
[d]Estimated from the photometry up to the Q band given by Wilking et al. (1986).

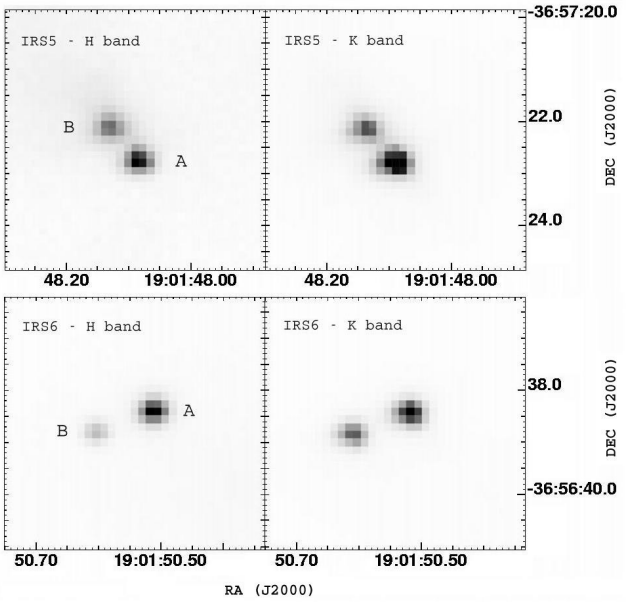

Fig. 1. VLT-ISAAC H and K images of the sources IRS5 and IRS6 were the discovered binary components a and b are indicated.

medium resolution spectra were also acquired in two spectral segments centered at 2.261 μm and 2.161 μm each covering ∼0.122 μm around the central wavelength. HH100 IR, IRS2 and IRS3 were also observed in an additional segment in the H band, centered at 1.6295 μm and covering ∼0.080 μm. For these observations we used the 0.″3 slit correspondig to a nominal resolution of $R \sim 8000$ and $R \sim 9000$ for the K and H observations, respectively. Spectra of standard stars of spectral type O were also obtained at both low and medium resolution at an airmass similar to the scientific spectra to correct for telluric absorption. The telluric spectra were carefully cleaned of any intrinsic HI and He absorption feature before being used. In the low resolution spectra, wavelength calibrations were performed using a Xenon lamp spectrum taken at the end of the night. At medium resolution, the lamp calibration was refined each time on the OH sky lines observed in the spectra. In addition, the object and standard spectra were carefully aligned with each other against the atmospheric absorption features before being divided. This procedure leads to a wavelength calibration error in medium resolution mode that we estimated to be of the order of 0.1 Å (i.e. about 1−2 km s^{-1}).

The spectra were obtained during non-photometric nights, with a seeing varying between 1.5 and 2 arcsec. To flux calibrate our spectra we therefore used the broad band photometry obtained at SOFI with the NTT instrument during March 2003, whose values are reported in Table 1. For IRS5 and IRS6, since the NTT resolution is not high enough to resolve the binaries, we derived the magnitudes of the relative components using H and K VLT-ISAAC images taken from the ESO archive (ID programme 63.I-0691, April 1999). These are also reported in Table 1. From this table, and from the comparison of our derived photometry with the photometry given by Taylor & Storey (1984), we notice that a certain degree of variability is present in the considered sources, with the largest variation exhibited by HH100 IR and IRS3. HH100 IR was already known to be highly variable, with near IR magnitudes changing by values more than two magnitudes on timescales of one year (Molinari et al. 1993).

The complete low resolution spectra of the targetted sources are shown in Fig. 2. The NIR SEDs of all the sources but IRS3 are characterized by a continuum steeply rising from the J to the K band. The IRS 3 SED peaks in the H band and then declines. This evidence, and the fact that the more recently measured $H-K$ color of this source is smaller by about 1 mag

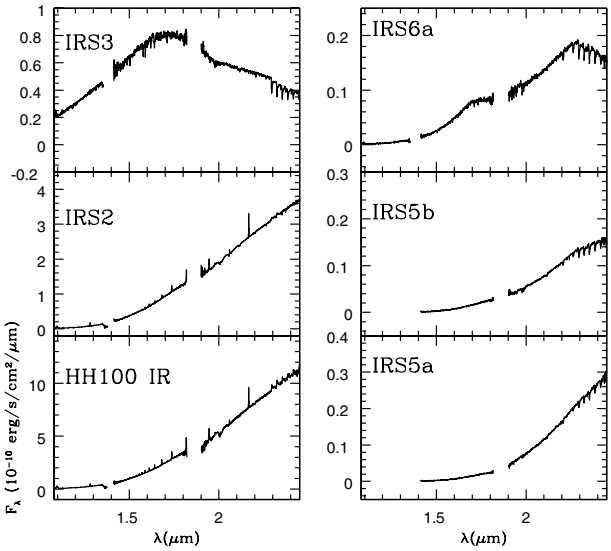

Fig. 2. Low resolution *J*, *H* and *K* spectra of the observed sources.

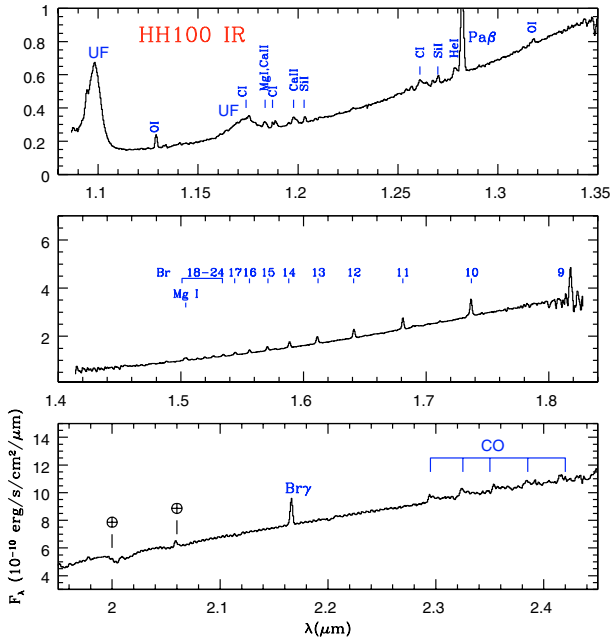

Fig. 3. Low resolution *J*, *H* and *K* spectra of HH100 IR with the main emission lines and features labelled.

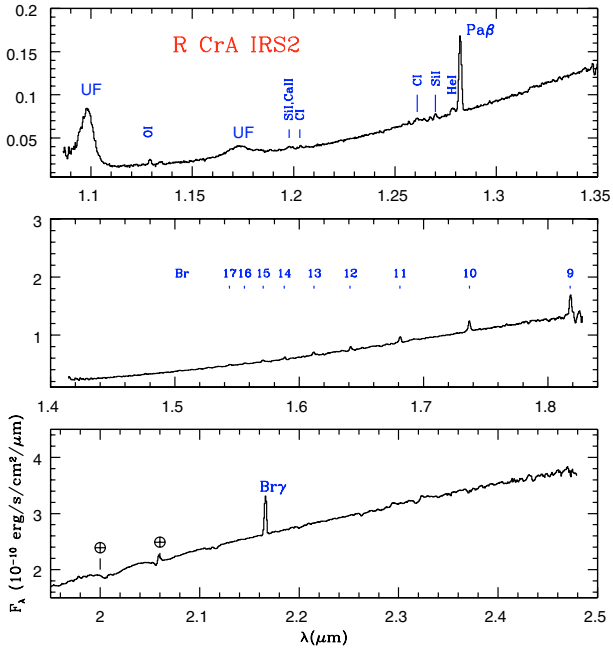

Fig. 4. Low resolution *J*, *H* and *K* spectra of IRS2 with the main emission lines and features labelled.

than the value given by Taylor & Storey (1984) (see Table 1), indicate that the IRS3 IR excess has been significantly reduced over time. In the low resolution spectra of IRS3, IRS5a,b and IRS6a some features in absorption are present, while no significant line is detected in emission. Conversely, IRS2 and HH100 IR are characterized by rich emission spectra with no absorption features (see also Figs. 3 and 4). Moreover in both of these spectra, and to a lesser extent also in IRS6a, we detect two broad features at ~1.10 and 1.17 μm which remain unidentified.

Figures 5–7 show the normalized, high resolution spectral segments observed in each source. Given the weakness of IRS5b with respect to the other component, it was not possible to extract its medium resolution spectrum and therefore only the MR spectrum of IRS5a has been analyzed. All these spectra are characterized by the presence of many features in absorption. This is true also for HH100 IR and IRS2 where the higher resolution has made it possible to detect narrow and weak features which remained undetected in the low resolution spectra. We will separately discuss the emission and absorption spectra of the observed sources in Sects. 4 and 5.

4. The emission lines

HH100 IR and IRS2 are the only sources showing a prominent emission spectrum rich in features (Figs. 3 and 4). Such features mainly include permitted transitions of neutral atoms. The HI lines are the strongest of these: we detect Brγ, Paβ and other lines from the Brackett series up to quantum number $n = 20$ in HH100 IR and IRS2, while weak Brγ emission has also been measured in the MR spectrum of IRS5a. The HI lines observed in HH100 IR have already been presented and discussed in Nisini et al. (2004); in Table 2 we report the fluxes and the kinematical properties of the HI lines detected both in the low and high resolution spectra of IRS2 and IRS5a. The Brackett decrement observed in HH100 IR is consistent with emission from moderately optically thick lines originating from a compact region of few stellar radii. Moreover, the fact that the Brackett line profiles observed in high resolution are almost symmetrical, with linewidths decreasing with the upper quantum number, is in favour of an origin in an expanding stellar wind rather than in an accretion region, as often suggested for these lines (e.g. Muzerolle et al. 1998). On this hypothesis, a mass loss rate of $\sim 10^{-6}$ $M_\odot\,\mathrm{yr}^{-1}$ has been derived for HH100 IR by using a simple model of an ionized wind (Nisini et al. 2004). The Brackett lines observed in IRS2 show characteristics similar to the HI lines of HH100 IR, such as symmetry of the Brγ line and large linewidths. The Br12 and 13 profiles

Table 2. Emission lines observed in HH100 IR and IRS2 (excluding HI lines).

λ_{obs}	$F(\Delta F)$	$F(\Delta F)$	Identification (λ_{vac} in μm)
μm	10^{-15} erg s^{-1} cm^{-2}		
	HH100 IR	IRS2	
1.1291	1.52(0.05)	0.89(0.07)	OI $3p^3P-3d^3D^0$ 1.1287
1.1327	0.05(0.05)	...	CI $3d^1D^0-3p^1P$ 1.1333
1.1339	0.15(0.05)	...	CI $3d^1F^0-3p^3D$ 1.1339
1.1641	0.34(0.08)	...	CI $3d^3D^0-3p^3D$ 1.1632, 1.1651
1.1754	0.59(0.08)	...	CI $3d^3F^0-3p^3D$1.1751,1.1756, 1.1758
1.1831	0.37(0.08)	...	MgI $4s^1S-4p^1P^0$ 1.1831
1.1839	0.55(0.08)	...	?
1.1835	0.84(0.08)	...	CaII $5p^2P^0-5s^2S$ 1.1842
1.1873	0.27(0.08)	...	?
1.1888	0.84(0.08)	0.27(0.06)	CI $4s^3P^0-3p^3D$1.1883
1.1954	0.32(0.05)	...	CaII $5p^2P^0-5s^2S$ 1.1953
1.1978	1.02(0.05)	0.83(0.06)	?
1.1992	0.81(0.05)	0.20(0.06)	SiI $4p^3D-4s^3P^0$ 1.9948
1.2035	0.60(0.05)	0.35(0.06)	SiI $4p^3D-4s^3P^0$ 1.2035
1.2086	0.19(0.05)	...	MgI $4f^1F^0-3d^1D$ 1.2087
1.2111	0.62(0.05)	...	SiI $4p^3D-4s^3P^0$ 1.2107
1.2275	0.30(0.04)	...	SiI $4p^3D-4s^3P^0$ 1.2274
1.2542	0.26(0.04)	...	
1.2568	0.36(0.04)	0.3(0.1)	CI $3d^3P^0-3p^3P$1.2566 +
			[FeII] $a^6D_{9/2}-a^4D_{7/2}$ 1.2567
1.2611	1.93(0.04)	1.6(0.1)	CI $3d^3P^0-3p^3P$1.2617
1.2640	0.93(0.04)	0.8(0.1)	FeII $z^6F_{7/2}-c^4F_{5/2}$ 1.2646
1.2675	0.60(0.04)	0.5(0.1)	?
1.2701	1.02(0.04)	1.0(0.1)	?
1.2784	1.18(0.04)	1.2(0.2)	?
1.3176	0.64(0.12)	...	OI $3p^3P-4s^3S^0$ 1.3166
1.4884	10.3(1.3)	...	MgI $4f^3F^0-3d^3D$ 1.4882
1.5047	20.1 (0.7)	3.5 (0.9)	MgI $4p^3P^0-4s^3S$ 1.5044 + Br23
1.7113	11.1(1.8)	...	MgI $4p^1P^0-4s^1S$ 1.7113
2.294	540(30)	87(17)	CO v = 2–0
2.324	600(30)	110(25)	CO v = 3–1
2.354	500(30)	...	CO v = 4–2
2.324	390(40)	...	CO v = 5–3
2.324	360(40)	...	CO v = 6–4

are also narrower than the Brγ line, but they appear less symmetric partly due to a superposition of few photospheric absorption lines which make it difficult to reconstruct the intrinsic line profile. The IRS2 Brackett decrement resulting after the observed lines have been de-reddened with an extinction value $A_V = 20$ (see Table 7) is compatible with line optical depths smaller than for HH100 IR (see e.g. Fig. 2 of Nisini et al. 2004), indicating lower densities of ionized material. If interpreted in the same wind model adopted for HH100 IR, such a decrement is consistent with a mass loss rate of ionized gas of $\sim 10^{-8}$ $M_\odot$ yr^{-1}, corresponding to a total mass loss rate of $\sim 1-2 \times 10^{-7}$ $M_\odot$ yr^{-1} assuming an ionization fraction between 0.05 and 0.1.

The other emission lines detected in the low resolution spectra of HH100 IR and IRS2 are listed in Table 3 where we have included only the features having an S/N larger than 3 and linewidth comparable to the instrumental resolution. In this table we indicate, when possible, the most probable identification made using the NIST database[1] and guided by the spectra of other YSOs (Kelly et al. 1994) or objects with likely similar excitation conditions (Walmsely et al. 2000;

[1] http://physics.nist.gov/PhysRefData/ASD1/

Table 3. HI lines in IRS2 and IRS5a.

Fluxes			
		IRS2	IRS5a
λ_{obs}	Line	$F(\Delta F)$	$F(\Delta F)$
μm		10^{-15} erg s^{-1} cm^{-2}	
1.282	Paβ	13.7(0.4)	
1.519	Br 20	1.6(0.5)	
1.527	Br 19	2.9(0.7)	
1.534	Br 18	3.7(1.1)	
1.544	Br 17	4.2(0.2)	
1.556	Br 16	4.1(0.4)	
1.571	Br 15	7.2(0.1)	
1.588	Br 14	6.0(0.7)	
1.612	Br 13	10.7(0.1)	
1.641	Br 12	9.3(0.6)	
1.681	Br 11	19.1(0.1)	
1.737	Br 10	41.5(0.9)	
1.818	Br 9	82.3(1.7)	
2.166	Brγ	181.0(5.4)	1.3(0.1)

Kinematical information					
		IRS2		IRS5a	
λ	Line	V_{LSR}	ΔV	V_{LSR}	ΔV
(μm)		km s^{-1}	km s^{-1}	km s^{-1}	km s^{-1}
1.6113	Br 13	-13 ± 4	130		
1.6411	Br 12	-11 ± 4	146		
2.1661	Brγ	-9 ± 4	180	0 ± 10	122

Hamann et al. 1994). We tried as much as possible to check the plausibility of a line identification by verifying that all the transitions of the same atom expected to originate from the same term were also detected. The observed atomic lines include several CI, OI, SiI and Mg I transitions, all coming from levels with energies <12.3 eV. The only ionic lines detected are from singly ionized Fe and Ca, which have ionization potential lower than 8 eV. In the high resolution spectral segments, in addition to the Brγ, Br12 and Br13 lines, the Na I doublet lines at 2.206 and 2.209 μm, and the 2.12 μm H_2 $v = 1-0$ S(1) lines are detected in emission in HH100 IR and IRS2 and their fluxes and kinematical characteristics are reported in Table 3.

Most of the observed atomic lines can be excited by both recombination and photo-excitation. For the two OI lines at 1.1287, 1.3165 μm fluorescence excitation by a UV continuum or resonant absorption of HI Lyβ photons have been proposed as the most likely excitation mechanisms (see e.g. Kelly et al. 1994; Walmsley 2000). The several CI lines are on the other hand the brightest permitted lines predicted by recombination theory (Escalante & Victor 1990). The several lines from SiI and MgI, which have low ionization potentials, may also originate from a recombination cascade. Some of the atomic species observed are those responsible for strong permitted optical lines in T Tauri stars, such as NaI and CaII. The levels from which the IR lines originate lie at excitation energies larger than the levels of the optical lines, but it is conceiveable that the origin of the emission must be similar. Among different possibilities, emission from the disk-star accretion region (Basri & Bertout 1989; Hartmann 1998), from a stellar wind (Hartmann et al. 1990) and from an active chromosphere (Calvet et al. 1984) are the most commonly proposed. The kinematical characteristics of the two Na I lines detected in high resolution are remarkably similar to those of the Brγ emission, both in terms of linewidth and V_{LSR}, which suggests that they come from the same emission region. We also note the absence of forbidden lines, e.g. from [FeII], which indicate that the emission line region is characterized by high densities where forbidden lines with critical densities lower than 10^5 cm^{-3} are quenched.

The weak H_2 2.12 μm line detected in HH100 IR and IRS2 (Table 4) may be an indicator of both shocked gas in the interaction of the stellar wind with the ambient medium, and emission from the inner warm region of a circumstellar disk. The line is blueshifted and only barely resolved, with an intrinsic width of $\lesssim$20 km s^{-1}. Given these characteristics, the detected H_2 emission may trace the base of a compact molecular outflow, such as those already detected in other Class I sources by Davis et al. (2001). In our case the emission is not spatially resolved, however the adopted slit may not be aligned with the compact jet emission. The origin in a circumstellar disk is, however, equally plausible. The upper limit on the line widths together with the source mass estimates given in Table 7 indicate that for a Keplerian disk the observed line are consistent with an emission region at >1 AU from the stellar source. Ro-vibrational H_2 emission with linewidths similar to those observed by us have been detected from disks of some T Tauri stars (Bary et al. 2003). In conclusion both the jet and the disk hypothesis seem to be plausible for the 2.12 μm line origin. Finally CO in emission from different vibrational band heads in the 2.3 μm region is also detected in HH100 IR and IRS2. CO band head emission is a tracer for dense molecular gas at $T \sim$ 2000–3000 K, and it is usually interpreted as a sign of the presence of active accretion disks. The reason is that to have this band in emission large columns of warm gas need to be present, and accretion may represent a viable disk heating mechanism (Najita et al. 1996).

The spectra of HH100 IR, IRS2 and IRS6a show, in addition to the emission lines, two broad and strong unidentified features in emission, at 1.098 and 1.173 μm, whose parameters are given in Table 5. Such features do not seem to originate from spurious or instrumental effects since they are not observed either in the IRS3 spectrum or in the spectra of the standard stars. They do not appear spatially resolved along the slit, being confined on the source. The large widths and strengths of these features bring to mind the characteristic shape of PAH emission, which however have never yet been observed at these wavelengths. The observations of PAHs at such short wavelengths would imply electronic excitation of these macromolecules and consequently the presence of strong UV fields which do not seem to be associated with the low luminosity sources we are considering. The attribution of these features

Table 4. Other emission lines in the high resolution spectra.

		HH100 IR			IRS2		
λ	Line	$V_{\rm LSR}$	ΔV	$F \pm \Delta F$	$V_{\rm LSR}$	ΔV	$F \pm \Delta F$
μm		km s^{-1}	km s^{-1}	10^{-17} erg s^{-1} cm^{-2}	km s^{-1}	km s^{-1}	10^{-17} erg s^{-1} cm^{-2}
2.1218	H_2	–6	$\lesssim$20	5.4 ± 0.3	–6	$\lesssim$20	3.4 ± 1.0
2.2062	Na I $^2P^0_{3/2}$–$^2S_{1/2}$	5	142	32.0 ± 0.8	...	...	8.8 ± 1.5
2.2090	Na I $^2P^0_{1/2}$–$^2S_{1/2}$	2	133	42.0 ± 1.5	−11	117	19.0 ± 0.5

Table 5. Parameters of the 1.1 μm unidentified features.

	HH100 IR		IRS2	
λ	$F \pm \Delta F$	*FWHM*	$F \pm \Delta F$	*FWHM*
μm	10^{-14} erg s^{-1} cm^{-2}	μm	10^{-14} erg s^{-1} cm^{-2}	μm
1.098	42.9 ± 0.9	7.4×10^{-3}	5.1 ± 0.2	7.5×10^{-3}
1.173	13.2 ± 0.7	1.3×10^{-2}	1.4 ± 0.1	1.2×10^{-2}

to PAH emission is also not favoured by the non-detection of the vibrationally excited PAH feature at 3.3 μm in the spectrum of HH100 IR (Whittet et al. 1996). Diffuse interstellar bands (DIBs) have been detected in the spectral range considered (Joblin et al. 1990) but they are features usually observed in absorption against a strong continuum. Finally, unidentified dust emission features at 1.15 and 1.5 μm have been observed towards the reflection nebula NGC 7023 (Gordon et al. 2000). Such features are however much broader (∼0.2−0.3 μm) and more diffuse than those detected by us.

5. The absorption features

In the two *K* band spectral segments, the main absorption features observed are those of lines from neutral atoms like Na, Al, Fe, Mg, Ti and Si, as well as the CO 2−0 band; these are the typical features expected from the photosphere of late type (K-M) stars (e.g. Wallace & Hinkle 1996, 1997) and commonly observed in pre-main sequence sources (e.g. Luhman & Rieke 1998). In HH100 IR and IRS2 such features are detected at only 1−5% of the continuum level. In the *H* band spectral segment, several more features are detected, most of which are very weak. The most significant of these features are indicated in Figs. 5−7 and have been identified through the spectra of standard stars of Meyer et al. (1998) and the Kurucz atomic spectral line database[2]. The absorption lines are resolved, with widths of several tens km s^{-1} which vary depending on the considered feature in the same objects. Such a broadening is due to different contributions, including rotation and Zeeman broadening, since these young stars are expected to be fast rotators and to have strong stellar magnetic fields. More specifically, the width of lines selected for having small Landé factors and not being blended with other features are of the order of ∼20 km s^{-1} in IRS3, 40 km s^{-1} in IRS2, HH100IR and IRS6a, and 60 km s^{-1} in IRS5a. This indicates that all the sources but IRS3 possess large v sin i values, comparable with the projected rotational velocities estimated in other flat-spectrum and Class I sources and higher than the average v sin i values measured in T Tauri stars ($\langle v \sin i \rangle \sim 15$ km s^{-1} , Bouvier et al. 1986).

[2] 1995 Atomic Line Data (R.L. Kurucz and B. Bell) Kurucz CD-ROM No. 23. Cambridge, Mass.: Smithsonian Astrophysical Observatory.

5.1. Spectral type and veiling measurement

On the assumption that the observed absorption lines originate from the stellar photosphere, their equivalent widths (EWs) should be sensitive to the stellar effective temperature and gravity. In the sources we are considering, however, the line EWs are strongly affected by the presence of continuum excesses, which can be quantified through the *veiling* parameter, defined as the flux at a given wavelength in excess over the photospheric flux ($r_\lambda = F_{{\rm ex},\lambda}/F_{*,\lambda}$). The veiling is actually a parameter that we also want to derive from the data, as it gives us information on the circumstellar activity of the stars. The ratios of different lines close in wavelength is not largely affected by the veiling and can thus be used for defining the spectral type. Then, the absolute value of the line EWs can be in turn compared with the intrinsic EW of spectral standard lines to estimate the IR veiling. Several diagnostic lines, mainly located in the *K* band, have been identified by different authors as particulary suited for spectral classification (e.g. Luhman & Rieke 1998). Among them, different features lying in the region around the Na I doublet at 2.206 μm are good diagnostic tools for the effective temperature, while the CO 2−0 bandhead is particularly sensitive to the gravity (e.g. Doppmann & Jaffe 2003). However, we have seen that in HH100 IR and IRS2 both the Na I doublet lines and the CO band-heads are seen in emission instead of absorption, and therefore cannot be used for spectral classification. Therefore, to derive the stellar properties of our sources, we have used different diagnostic lines close in wavelength, mainly located in the *K* band. Details for the lines are given in Appendix A. In practice to derive the

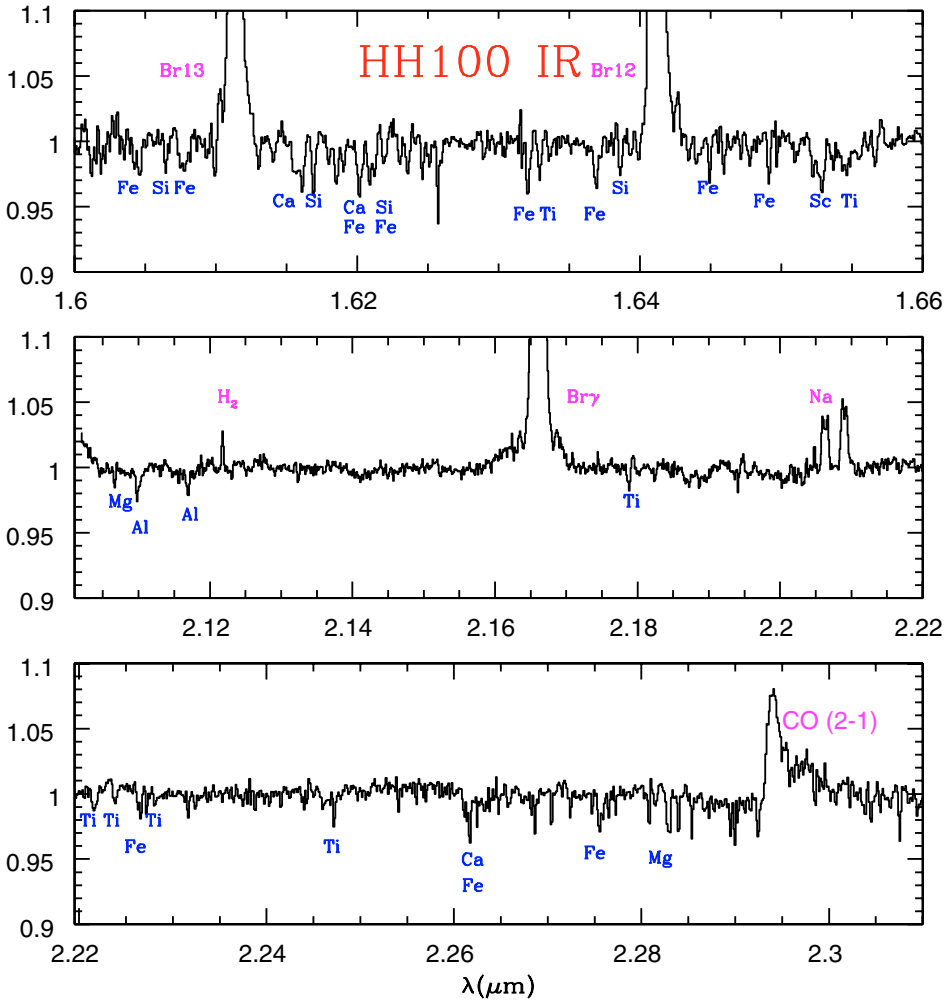

Fig. 5. Continuum normalized, medium resolution spectra of HH100 IR. The most important emission and absorption features are labelled.

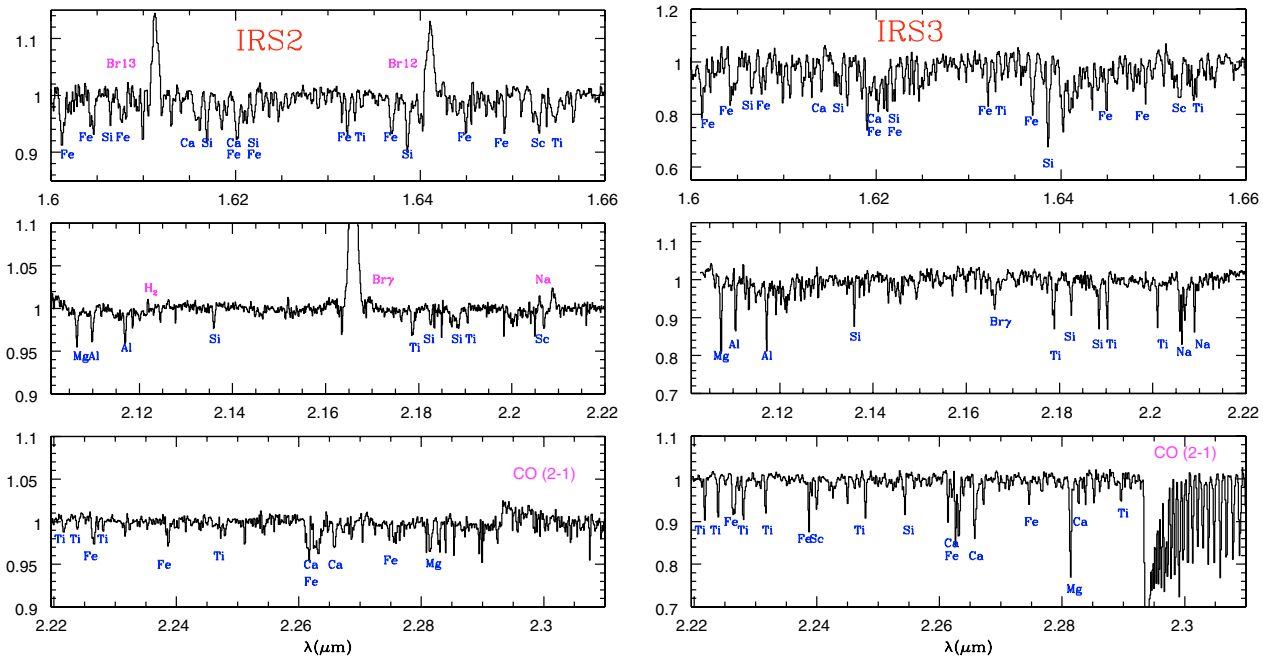

Fig. 6. As in Fig. 5 but for IRS2 (*left*) and IRS3 (*right*).

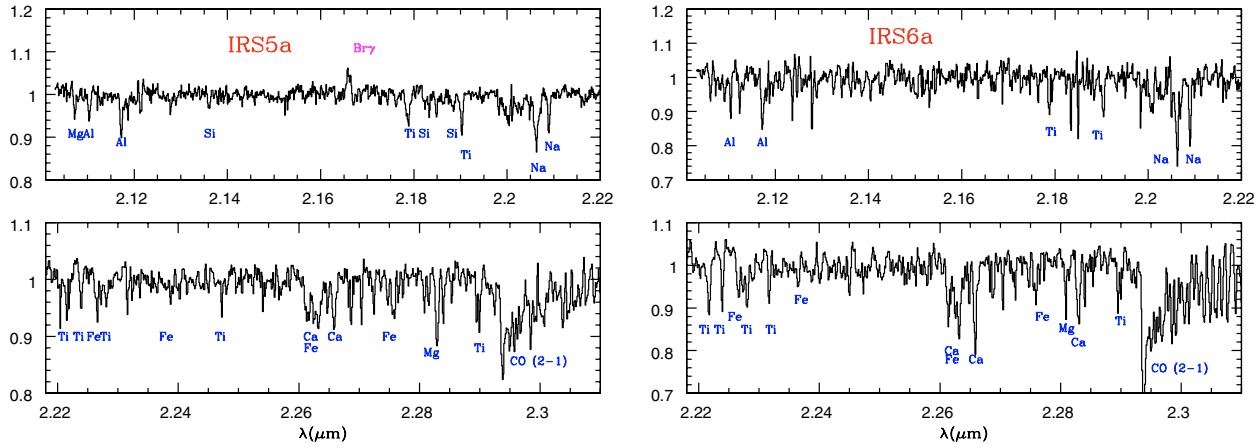

Fig. 7. As in Fig. 5 but for IRS5a (*left*) and IRS6a (*right*).

spectral type and luminosity class, we have compared the ratios of selected absorption lines observed in our sources with the same ratios as measured in a grid of standard star spectra, selecting the standard which minimizes the scatter among the different ratios.

A difficulty in this procedure is caused by the limited number of available spectra of standard stars at a resolution similar to that adopted for our observations. For our analysis we have mainly used the Wallace & Hinkle (1997) (for K band), and Meyer et al. (1998) (for the H band) standard samples, which are however at resolution 3000, thus not always making it possible to compare lines resolved in our spectra but blended in the standard stars spectra. Moreover, the Wallace & Hinkle (1997) sample lacks spectra of dwarf stars between K5 and M 2. We therefore also used the dwarf standard star spectra obtained by Greene & Lada (2002) which have a finer grid between K4V and M2V at a resolution of about 15 000, but do not entirely overlap with our observed spectral range.

The spectral types and luminosity classes derived for the sources of our sample using the procedure described above are given in Table 6. The effective temperatures $T_{\rm eff}$ relative to each spectral type have been derived adopting the conversion of spectral type into $T_{\rm eff}$ given in Kenyon & Hartmann (1995). We estimate that our classification is correct within one spectral sub-class, with the exception of HH100 IR where the paucity and weakness of the absorption features do not allow a classification better than within two spectral sub-classes. Figures 8−10 show a comparison between the spectra of our sources and the spectra of standard stars which more closely match the observed spectra. Most of the sources are consistent with being dwarfs, as has been also found for other low mass YSOs (i.e. Greene & Lada 1997). The dwarf spectra shown by young stars have been recognized as evidence for the observed features originating in the stellar photosphere rather than in a circumstellar disk. Disk photospheres are indeed expected to have low gravity and thus their spectra should resemble those of giant or supergiant stars (Greene & Lada 1997).

Once the spectral type has been defined, the measured EWs of selected lines, compared with the EWs of standard spectra of the corresponding spectral type, have been used to derive the veiling in the K and H band. For this purpose we used lines not blended at the lower resolution of the available standard spectra, and not contaminated by possible spurious atmospheric feature residuals. We also selected lines not too sensitive to the effective temperature to minimize the uncertainty in the spectral type determination and also not too sensitive to the effect of stellar magnetic fields, like the Ti lines at 2.23 μm whose EW can be increased by the Zeeman effect due to their high Landé factor (e.g. Johns-Krull & Valenti 2000). In practice, good lines for the veiling determination were found to be, in addition to the Na line at 2.209 μm when observed in absorption, Al at 2.1099 μm and Ca at 2.2658 μm for the K band, and Fe (1.6369 μm) and Si(1.6386 μm) in the H band. For IRS5a and IRS6a we do not have the medium resolution H band spectra, but a few absorption features are detected in their low resolution spectra. Among them, Mg I at 1.7112 μm is the most suited to evaluate the H veiling, not being affected by strong blending even at low resolution.

Table 6. Spectral types and veiling.

Source	ST	$T_{\rm eff}$	r_K	r_H
IRS2	K2V	4900 ± 200	2.9 ± 0.5	1.4 ± 0.2
IRS5a	K5-K7V	4200 ± 200	1.0 ± 0.1	0.1 ± 0.1
IRS6a	M2V	3580 ± 100	0.1 ± 0.1	0.1 ± 0.1
HH100 IR	K5-M0V	4060 ± 300	6.0 ± 0.5	3.5 ± 0.2
IRS3	K5-M0 III	3800 ± 100	0.2 ± 0.1	0.1 ± 0.1

The resulted veiling values are also listed in Table 6. From the table it can be seen that, as expected, HH100 IR and IRS2 have the largest veiling values, $r_K \sim 6$ and 3 respectively. The other considered sources show lower or zero veiling values. Finally, the veiling in the H band is about a factor of two smaller than the r_K value. These veiling determinations will be discussed in Sect. 7.3.

6. Stellar and circumstellar parameters

The derivation of spectral type and veiling allows us to estimate other stellar and circumstellar properties from the available K and H photometry and source bolometric luminosity.

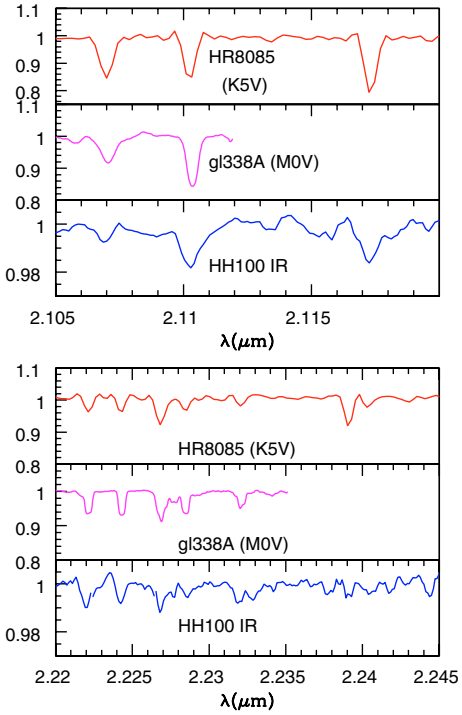

Fig. 8. Normalized spectral segments of HH100 IR in the K band compared with the spectra of K5V (Wallace & Hinkle 1997) and M0V (Greene & Lada 2001) standard stars.

The infrared color excess $E(H-K)$ can be derived from the observed $(H-K)$ color, the star color relative to the adopted spectral type $(H-K)_*$ and the r_K and r_H values:

$$E(H-K) = (H-K) - (H-K)_0, \quad (1)$$

$$(H-K)_0 = (H-K)_* - 2.5 \log\left(\frac{1+r_H}{1+r_K}\right) \quad (2)$$

where we have indicated by $(H-K)_0$ the dereddened IR color of the source. From this expression the visual extinction has been evaluated adopting $A_V = 15.9\,E(H-K)$ given by the standard interstellar reddening law (Rieke & Lebofsky 1985). The derived values are listed in Table 7 and range from A_V = 10 mag in IRS3 to A_V = 45 mag in IRS5a. Our derived values for HH100 IR, IRS2 and IRS5 compare rather well with the extinction derived in these sources from the optical depth of the 10 μm silicate and 3 μm water absorption features, i.e. ∼25−30 mag for HH100 IR, 27 mag for IRS2 and 45 mag for IRS5(a+b) (Chen & Graham 1993; Whittet et al. 1996). The low extinction value (∼10 mag) derived for IRS3 is consistent with values found towards field stars obscured by the R CrA cloud (Whittet et al. 1996). From the adopted spectral type and from the K magnitude dereddened by the derived A_V value, we are now able to derive the absolute stellar K magnitude, and thus the intrinsic stellar luminosity:

$$\log L_*/L_\odot = -0.4(M_{bol} - M_{bol,\odot}), \quad (3)$$

where

$$M_{bol} = BC + M_K + (V-K)_*. \quad (4)$$

In this expression the values for the bolometric correction BC and for the intrinsic stellar $(V-K)_*$ colors for dwarfs were taken from Kenyon & Hartmann (1995). Finally, the stellar radius R_* can be also derived given the assumed stellar effective temperature. Table 7 lists the L_* and R_* values for the five considered sources. Luminosities range between 0.3 and 4.3 $L_\odot$, and stellar radii between 1.2 and 3.6 $R_\odot$, being therefore in the range expected for low mass young stars (e.g. Siess et al. 1997). Given the stellar luminosity and its effective temperature, the sources can be positioned in a HR diagram so as to have an estimate of their masses and ages through the comparison with pre-main sequence evolutionary tracks. This is shown in Fig. 11, where we have considered the D'Antona & Mazzitelli (1997) tracks for stars with masses between 0.1 and 2 $M_\odot$. From these tracks we derive masses between 0.3 and 1 $M_\odot$ and ages between 10^5 and 10^6 yr. In order to check for the sensitivity of the different models used to derive the evolutionary tracks, we have also derived masses and ages adopting the Siess et al. (2000) models, which are listed in Table 7. These last models give slightly higher masses and ages than the D'Antona & Mazzitelli tracks, with mass variations which are about 80% at worst. The considered standard tracks do not take into account the perturbation introduced in the evolutionary tracks by a high mass accretion rate, an effect which might be not negligible for HH100 IR and IRS2. Siess et al. (1997, 1999) have computed evolutionary tracks for stars which are still accreting a substantial fraction of their mass; they evaluated the error introduced in the mass and age determination by taking the values expected for standard tracks. They show that while the determination of the (current) mass is not very strongly affected by a high accretion rate, the stars that are still accreting are younger than the standard ones, for ages $\lesssim 1.5\times10^6$ yr. Thus, it is likely that HH100 IR and IRS2 are actually younger than the age of $\sim 5\times10^5$ and 10^6 yr, respectively, that we infer from the tracks in Fig. 11.

The knowledge of the intrinsic stellar luminosity allows us in principle to derive what is the fraction of excess luminosity due to accretion through a comparison with the source bolometric luminosity. The error in this L_{acc} determination is largely dominated by the precision through which the L_{bol} value is known. L_{bol} values estimated through near IR and IRAS photometric data are given for HH100 IR, IRS2 and for IRS5 (Wilkings 1986, 1992, see Table 1). IRS5a is brighter and its near IR specrum is steeper than IRS5b, which suggests that the bolometric luminosity of IRS5a dominates over the binary system: we assume a ratio 2:1 to distribute the L_{bol} value between the two components. For IRS6 and IRS3 measurements of the far IR fluxes are not available; however the fact that their IR spectra are not very steep allow us to assume that the far IR contribution at the L_{bol} value can be negligible. We have therefore given an estimate of the L_{bol} values for these sources based on their near and mid IR ground based photometry, and adding a correction which assumes that the spectrum scales as the wavelength for λ larger than that corresponding to the last observed photometric flux. For IRS6 we further assumed that the two components a and b contribute equally to the total bolometric luminosity.

From the comparison of the derived stellar luminosity with the L_{bol} values, it appears that only HH100 IR and IRS2 have

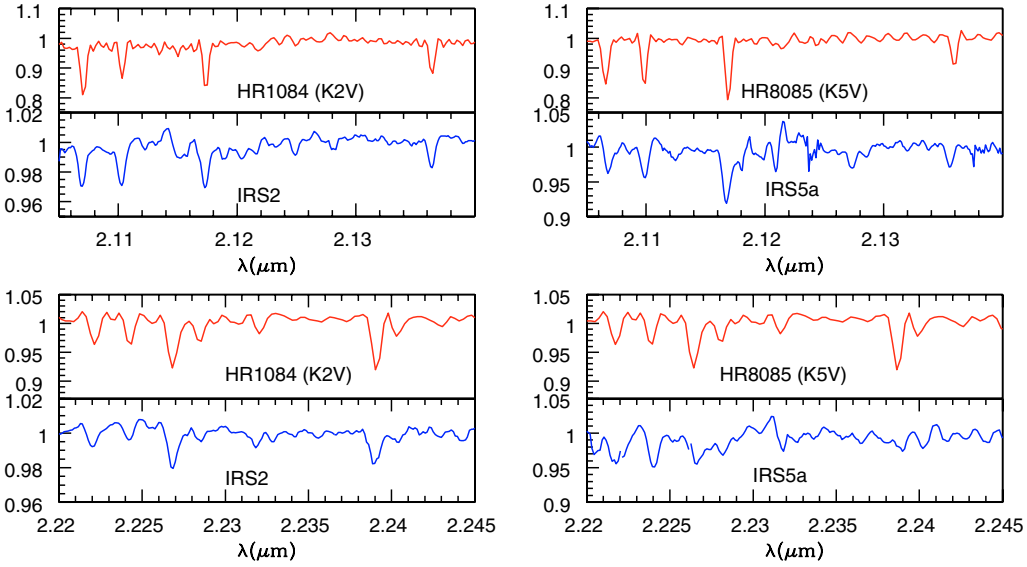

Fig. 9. Normalized spectral segments of IRS2 (*left*) and IRS5 (*right*) in the *K* band compared with the spectrum of the standard star which best matches the observations. The observed spectra have been rebinned at the resolution of the standard (~3000) for comparison.

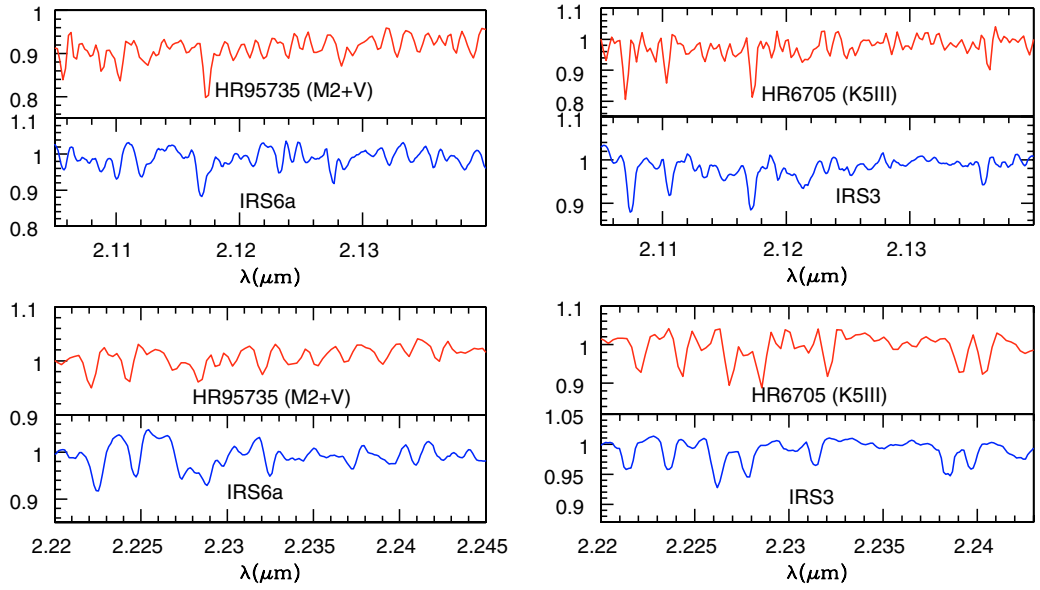

Fig. 10. Normalized spectral segments of IRS6 (*left*) and IRS3 (*right*) in the *K* band compared with the spectrum of the standard star which better match the observations. The observed spectra have been rebinned at the resolution of the standard (~3000) for comparison.

a significant excess of luminosity with respect to L_*, which amounts to 80% and 65% of the $L_{\rm bol}$ value, respectively. We attribute this extra luminosity contribution to the energy released in the accretion process. In IRS5a, only ~20% of the total luminosity is due to accretion while in the other two sources our method does not allow us to measure any significant accretion luminosity. Finally, the mass accretion rate can be estimated from the accretion luminosity. In the hypothesis that accretion occurs through the circumstellar disk, the total disk accretion luminosity can be written as (Gullbring et al. 1998):

$$L_{\rm acc} \sim G\frac{M_*\dot{M}}{R_*}\left(1-\frac{R_*}{R_{\rm i}}\right) \quad (5)$$

where R_i is the inner disk truncation radius which is predicted to be of the order of $3{-}5R_*$. The $\dot{M}$ values for HH100 IR and IRS2 are $\sim 2\times10^{-6}$ and 3×10^{-7} $M_\odot$ yr^{-1}, respectively. Such values are larger than the average values derived for T Tauri stars by means of UV excess measurements (Gullbring et al. 1998), but lower than the values indirectly estimated in Class 0 sources through their mass loss phenomena, indicating that an evolution in the mass accretion rate during the protostellar life is indeed very likely.

7. Discussion

The ability to separately estimate the stellar and circumstellar properties of embedded YSOs gives the possibility to infer in better detail the evolutionary properties of these sources, to analyse their similarities with optically visible T Tauri stars in terms of veiling and accretion activity and finally to address

Table 7. Stellar parameters.

Source	L_*	R_*	M_*	Age	$E(H-K)$	A_V	L_{acc}	$\dot{M}_{acc}$
	$L_\odot$	$R_\odot$	$M_\odot$	$\times 10^6$ yr		mag	$L_\odot$	$M_\odot$ yr^{-1}
IRS2	4.3 ± 1.5	2.9 ± 0.6	1.4 ± 0.3[a]	0.5–1[a]	1.3 ± 0.2	20 ± 3	7.7 ± 2.5	3×10^{-7}[a]
			1.8[b]	2[b]				2×10^{-7}[b]
IRS5a	1.6 ± 0.5	2.4 ± 0.4	0.5 ± 0.1[a]	0.3–0.5[a]	2.9 ± 0.2	45 ± 3	~0.4	$\sim3\times10^{-8}$[a]
			0.9[b]	1.3[b]				$\sim2\times10^{-8}$[b]
IRS6a	0.5 ± 0.2	1.5 ± 0.3	0.3 ± 0.1[a]	0.5–1[a]	1.9 ± 0.3	29 ± 5	<0.1	$<5\times10^{-9}$
			0.4[b]	1.8[b]				
HH100 IR	3.1 ± 0.9	3.6 ± 0.7	0.4 ± 0.1[a]	0.1[a]	1.9 ± 0.2	30 ± 3	12 ± 2	2×10^{-6}[a]
			0.75[b]	0.6[b]				1×10^{-6}[b]
IRS3	0.3 ± 0.1	1.2 ± 0.1	0.5 ± 0.1[a]	1–5[a]	0.2 ± 0.2	10 ± 3	<0.1	...
			0.5[b]	4[b]				

[a] Masses and ages derived from the D'Antona & Mazzitelli (1997) tracks.
[b] Masses and ages derived from the Siess et al. (2000) tracks.

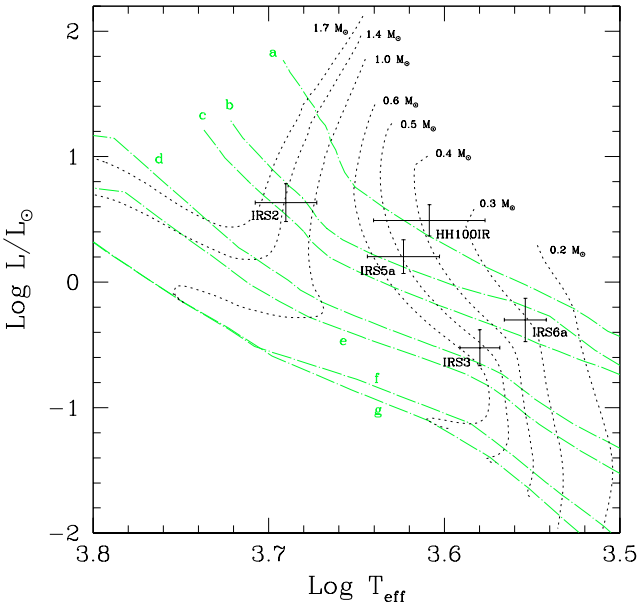

Fig. 11. HR digram of the R CrA sources with T_{eff} and stellar luminosity derived from the analysis of the medium resolution IR spectra. Evolutionary tracks (short dashed lines) and isochrones (dot-dashed lines) from D'Antona & Mazzitelli (1997) are shown for stellar masses between 0.2 and 1.7 $M_\odot$. Isochrones are reported for **a)** 10^5 yr, **b)** 5×10^5 yr, **c)** 10^6 yr, **d)** 5×10^6 yr, **e)** 10^7 yr, **f)** 5×10^7 yr and **g)** 10^8 yr.

quantitatively how their accretion properties are connected to other related phenomena such as jets and winds.

7.1. Evolutionary stage of the observed sources

The stellar parameters, accretion luminosity and mass accretion rates derived from the analysis of the star photospheric features can be used to assess the relative evolutionary phases of the observed sources. We have seen that only HH100 IR and IRS2 have a significant fraction of their luminosity due to accretion, which is also correlated with the presence of both extreme values for the K and H veilings and emission line activity. On the other hand, IRS5a, which like HH100 IR and IRS2 has been classified as a Class I protostar on the basis of its SED between 2 and 10 μm (Wilkings et al. 1997) does not show significant accretion activity, as testified by the low L_{acc}/L_{bol}, the absence of emission lines and the low veiling. Presumably this source is a T Tauri still embedded in its parental envelope or seen on an unfavourable line of sight. Finally, IRS6a and IRS3 present characteristics of pure reddened photospheres where there is little or no sign of activity connected to accretion. This analysis shows that YSOs chosen to have broadly similar IR colors may have very different accretion properties. This finding suggests that we should take an a posteriori look at the distribution of the IR colors of the considered sources to search for a finer separation between stars with different accretion properties. In particular the protostars HH100 IR and IRS2, having more than 50% of their luminosity due to accretion, are located, in a near IR color–color diagram, in a region defined by $(J-H) \gtrsim 4$ and $(H-K) \gtrsim 2.5$. The only other so far identified highly accreting protostar, i.e. YLW15 of the ρ Ophiucus cloud ($(J-H) > 5$, $(H-K) = 3.8$, Greene & Lada 2002), can be put in the same region. Sources with littel or no accretion activity (IRS6 and IRS3) seem to be located outside this box, with colors $(J-H) < 4$ and $(H-K) < 2.5$. In this scheme IRS5a is a borderline case, which remains anomalous. We only note that the colors of IRS5(a+b) are considerably bluer than those of the other highly accreting protostars ($(H-K)/(J-H) = 0.85$ vs. $(H-K)/(J-H) \sim 0.6$–0.7), indicating that part of its infrared excess may be due to scattered radiation. In conclusion we suggest that the real accreting protostars can be located in a color–color diagram region tighter than the previously considered locus for Class I sources (e.g. Lada & Adams 1992), a clue which deserves to be further investigated on the basis of a larger sample.

It is also interesting to note how the different accretion properties of the sources correlate with their position in the HR diagram. HH100 IR is the youngest source of the sample with an age $\lesssim 10^5$ yr, while all the others fall roughly on

the same isochrone at $t \sim 5 \times 10^5$–10^6 yr. If taken literally, this result indicates that sources with nearly the same age may have very different $L_{\rm acc}/L_{\rm bol}$ values, and thus that age is not the only parameter regulating the end of the accretion process. In particular, notice the different estimated mass accretion rate of sources (IRS2, IRS5a and IRS6a) which appear to have a similar age but different masses, ranging from ∼0.5 to ∼1.5 $M_\odot$. For these sources there is evidence that the mass accretion rate increases with the mass. Since the sources belong to the same star-forming core, they should have started to collapse with the same initial cloud infall rate, which depends only on the core kinetic temperature. Therefore, it is not unexpected that to accumulate a different mass in the same length of time, their mass accretion rate should have followed a different time evolution. Evidence for a correlation between mass accretion and stellar masses has indeed been reported, although with a broad scatter, for large samples of T Tauri and very low mass objects (Natta et al. 2004).

On the other hand, we should also recall that some of the stars considered have a large photometric variability as is indeed common in young embedded stars (e.g. Kaas 1999; Horrobin et al. 1997). Often variability at IR magnitudes is associated to variability of spectral features, such as HI and CO lines, whose emission is directly related to accretion (Biscaya et al. 1997; Nisini et al. 1994). Therefore, if the photometric variability of the considered sources is related to changes of the mass accretion rates on short timescales, as happens, e.g., in FU Ori-like events, the possibility that the three sources with the same age may have a similar *time averaged* mass accretion rate, cannot be excluded.

7.2. Origin of veiling

The observed sources present very different values of IR veiling. The K veiling values range from almost 0 in IRS3 and IRS6a, to ∼6 in HH100 IR. In T Tauri sources, r_K are normally estimated to be between 0 and 2 (Johns-Krull & Valenti 2001; Folha & Emerson 1999). Higher values, up to 3–4, have been measured in flat-spectrum and Class I objects (Greene & Lada 1997; Doppmann et al. 2003). However, we do not find a clear correlation with the class of the objects, at least for the three Class I sources of our sample which have r_K values of 0.5 (IRS5a), 3 (IRS2) and 6 (HH100) despite their similar spectral index between 2 and 10 μm. Instead, for these three sources the correlation with the estimated accretion luminosity is clearer. In T Tauri stars, the main considered source of IR veiling is the emission from the accretion disk, although, given their estimated low mass accretion rates, disk models find some difficulty in predicting the largest observed veiling values ($r_K \sim 1$–2) (Folha & Emerson 1999; Johns-Krull & Valenti 2001). The same models also have difficulty in reproducing the large IR veiling estimated in Class I sources, despite the mass accretion rate being higher than in T Tauri stars (e.g. Greene & Lada 1996). An additional source of veiling can be the emission from the inner circumstellar dusty envelopes. Greene & Lada (2002) estimate that the inner infalling envelope can account for about half of the K veiling they measure in the Class I object YLW15. Calvet et al. (1997), estimate that the thermal emission of envelopes with mass infall rates ranging from 10^{-5} to 4×10^{-6} $M_\odot\,{\rm yr}^{-1}$ can account for a 2.2 μm veiling ranging between 3 and 9, thus in the range of the values we find for HH100 IR and IRS2. The same models predict a H band veiling ∼30–50% smaller than in the K band, consistent with our derived values. Finally, the small veiling observed in IRS5a, despite its significant IR emission excess, can be explained by assuming that its envelope emission is mainly due to scattering of the emission of the central object. In this case, as pointed out by Calvet et al. (1997), the envelope flux contains the same spectral features as the object and thus does not affect the line EWs. Recent models for the SEDs of YSOs (Whitney et al. 2003) show that in Class II sources seen close to edge-on extinction and scattering dominate at near-IR wavelengths making the SEDs of these sources similar to those of less evolved Class I objects.

7.3. Correlation with accretion and ejection activity

Our observations show that HH100 IR and IRS2, most of whose luminosity is due to accretion, are also those exhibiting a rich emission line spectrum, with the strongest lines observed in the source with the highest mass accretion rate (HH100 IR).

Correlations between the accretion luminosity and the IR hydrogen line luminosity have been found in T Tauri stars (Muzerolle et al. 1998). Such a correlation can be naturally explained if the origin of HI lines is in the magnetospheric accretion region of the star but also if part of their emission comes from ionized outflows, which are ultimately powered by accretion. We can check if the highly accreting objects of our sample still follow the same correlation $L_{\rm acc} - L_{\rm Br\gamma}$ as T Tauri stars. Extending such a correlation to highly accreting embedded objects would indeed be important for validating the Brγ luminosity as an indirect quantitative tool for deriving the accretion luminosities of Class I sources. The Brγ luminosities of HH100 IR and IRS2, dereddened for the extinction values listed in Table 7, are 5.7×10^{-3} and 7×10^{-4} $L_\odot$, respectively. Following the fit derived by Muzerolle et al. (1998), such line luminosities should be consistent with accretion luminosities ∼40 and 3 $L_{\rm bol}$ respectively. Considering the large errors associated with the Muzerolle et al. least-squares fit, our derived $L_{\rm acc}$ values are consistent with the relationship found for the T Tauri stars, extending it to about an order of magnitude larger luminosities. Brγ emission is also observed in IRS5a with a luminosity value $\sim 5 \times 10^{-5}$ $L_\odot$. According to the relationship by Muzerolle et al. the corresponding $L_{\rm acc}$ value should be of the order of 10^{-1} $L_\odot$, well inside the locus of the T Tauri star and in agreement with our rough estimate value.

It is usually assumed that accretion and ejection of matter are correlated phenomena and that the latter is needed to remove part of the angular momentum carried by the accreting material. It is therefore worthwhile to see if a high accretion luminosity is always associated with the presence of outflows. In this respect it is indicative that HH100 IR is the only source of our sample that shows clear evidence of outflowing activity, being the identified exciting source of the HH100 Hebig

Haro nebulosity, and also of the HH objects HH101 (located in the SW) and HH99 (in the NE) (Hartigan & Graham 1987). A molecular bipolar outflow is also associated with this object as shown by the ammonia and HCO^+ observations of Anglada et al. (1989) and Anderson et al. (1997), respectively. IRS2, however, despite showing a large accretion luminosity value, does not show any undoubted tracer of mass ejection. We have seen that the weak H_2 2.12 μm line observed in emission can be due to both the outflow and the disk and no other lines typical of jets, such as [FeII] lines, are detected in the spectrum. On a larger scale no optical HH object seems to be associated to this source (Hartigan & Graham 1987). However, the region closer to IRS2 has not been investigated either in H_2 imaging, to search for molecular jets, or in molecular outflows radio tracers, so we cannot on this basis exclude that a large scale flow is associated with this source.

8. Conclusion

We have analyzed the low and medium resolution infrared spectra of a sample of embedded young stellar objects in the R CrA star-forming region with the aim of constraining their accretion properties and evolutionary stage. The sample includes three Class I sources (HH100 IR, IRS2 and IRS5) and two sources with NIR excesses in the Wilking et al. (1997) R CrA core survey (IRS6 and IRS3). The main results of this analysis are the following:

- The low resolution spectra revealed the presence of strong lines in emission only in two, namely HH100 IR and IRS2, out of the six observed sources. The most prominent detected features are permitted lines from neutral atoms, mostly from HI (Paβ, Brγ and lines from the Brackett series at higher-n) but also OI, NaI and CI. These lines arise in a partially ionized compact and very dense gas, likely originating either in the star-disk accretion region, or at the base of an expanding wind. The same sources where atomic lines are detected also show the CO 2.3 μm band-heads in emission, indicating the presence of large columns of warm molecular gas, probably located in the inner sections of an accretion disk. In the medium resolution spectra, also a weak H_2 2.12 μm line is detected in HH100 IR and IRS2, which may originate either in the circumstellar disk or in a molecular jet.
- The medium resolution spectra show plenty of absorbtion features typical of late-type stellar photospheres. In HH100 IR and IRS2 such features are very weak, indicating a large amount of IR veiling. We have derived the effective temperature, extinction, stellar luminosity and radius for each observed source, through a comparison with standard star spectra and IR photometric data. This information has been used in turn to infer the amount of IR veiling, the accretion luminosity and the mass accretion rate of each object.
- Only in HH100 IR and IRS2 does the accretion luminosity dominate over the total bolometric luminosity ($L_{\rm acc}/L_{\rm bol} \sim$ 0.8 and 0.6 respectively) and the derived mass accretion rates are of the order of 3×10^{-6} and 5×10^{-7} $M_\odot\,{\rm yr}^{-1}$ respectively, i.e. higher by an order of magnitude than the average values derived in T Tauri stars. In contrast, in IRS5a only ~2% of the luminosity is due to accretion. In general, we found that there is a correlation between the accretion luminosity, the IR veiling and the emission line activity of the sources.
- When compared with standard evolutionary tracks for pre-main sequence evolution, the derived stellar luminosities and effective temperatures indicate that HH100 IR is the youngest of the sources, with an age $\sim 10^5$ yr. On the other hand, IRS2, IRS5a and IRS6a have about the same age ($\sim 5 \times 10^5 - 10^6$ yr) despite the large differences in their accretion properties. For these sources there is a hint that the mass accretion rate, at a given age, may depend on the accumulated stellar mass, a result not totally unexpected if one assumes that the mass accretion rate is a function of the mass of the envelope. We cannot however exclude that variations on short timescales of the accretion rates, related to the sources infrared variability, may be responsible of the derived differences in the $\dot{M}$ values.

Our analysis has shown that sources broadly defined as Class I protostars may be very different in terms of accretion activity. This indicates how the definition of the evolutionary stage of deeply embedded YSOs by means of IR colors needs to be refined. In particular, on the basis of our results we suggest that the highly accreting protostars (i.e. those for which $L_{\rm acc}/L_{\rm bol} >$ 50%) can be located in a color−color diagram region characterized by near IR colors $(J-H) \gtrsim 4$ and $(H-K) \gtrsim 2.5$, a clue which remains to be further investigated for a larger sample. Low resolution IR spectroscopy can give a better diagnostic of the accretion activity of young embedded sources, evidenced by the presence of emission lines, HI recombination lines and CO overtone emission in particular. However, we have shown that the combination of low and high resolution spectroscopy may be effective in constraining both the stellar and circumstellar properties of even highly veiled objects, making it possible to directly derive the accretion luminosity and mass accretion rates back to the first 10^{-5} yr of protostellar evolution.

Acknowledgements. We thank Tom Greene for having kindly provided his NIRSPEC spectra of standards. We also thank Livia Origlia for useful discussions on spectral classification and Tom Geballe for helpful comments on the unidentified features. This research has made use of NASA's Astrophysics Data System Bibliographic Services and the SIMBAD database, operated at CDS, Strasbourg, France.

References

Alexander, R. D., Casali, M. M., André, P., Persi, P., & Eiroa, C. 2003, A&A, 401, 613
Anderson, I. M., Harju, J., Knee, L. B. G., & Haikala, L. K. 1997, A&A, 321, 575
Anglada, G., Rodriguez, L. F., Torrelles, J. M., et al. 1989, ApJ, 341, 208
Bacciotti, F., Mundt, R., Ray, T. P., et al. 2000, ApJ, 537, L49
Bary, J. S., Weintraub, D. A., & Kastner, J. H. 2003, ApJ, 586, 1136
Basri, G., & Bertout, C. 1989, ApJ, 341, 340
Biscaya, A. M., Rieke, G. H., Narayanan, G., Luhman, K. L., & Young, E. T. 1997, ApJ, 491, 359

Bontemps, S., André, P., Terebey, S., & Cabrit, S. 1996, A&A, 311, 858
Bouvier, J., Bertout, C., Benz, W., & Mayor, M. 1986, A&A, 154, 110
Burton, M. 1992, PASAu, 10, 52
Brooke, T. Y., Sellgren, K., & Geballe, T. R. 1999, ApJ, 517, 883
Calvet, N., Basri, G., & Kuhi, L. V. 1984, ApJ, 277, 725
Calvet, N., Hartmann, L., & Strom, S. E. 1997, ApJ, 481, 912
Chen, W. P., & Graham, J. A. 1993, ApJ, 409, 319
D'Antona, F., & Mazzitelli, I. 1997, in Cool stars in Clusters and Associations, ed. G. Micela, & R. Pallavicini, Mem. S. A. It., 68, 807
Davis, C. J., Ray, T. P., Desroches, L., & Aspin, C. 2001, MNRAS, 326, 524
Davis, C. J., Stern, L., Ray, T. P., & Chrysostomou, A. 2002, A&A, 382, 1021
Doppman, G. W., & Jaffe, D. T. 2003, AJ, 126, 3030
Doppman, G. W., Jaffe, D. T., & White, R. J. 2003, AJ, 126, 3043
Escalante, V., & Victor, G. A. 1990, ApJS, 73, 513
Fohla, D. F. M., & Emerson, J. P. 1999, A&A, 352, 517
Gordon, K. D., Witt, A. N., Rudy, R. J., et al. 2000, ApJ, 544, 859
Greene, T. P., & Lada, C. J. 1996, ApJ, 112, 2184
Greene, T. P., & Lada, C. J. 1997, AJ, 114, 2157
Greene, T. P., & Lada, C. J. 2002, AJ, 124, 2185
Gullbring, E., Hartmann, L., Briceño, C., & Calvet, N. 1998, ApJ, 492, 323
Joblin, C., Maillard, J. P., d'Hendecourt, L., & Leger, A. 1990, Nature, 346, 729
Johns-Krull, C. M., & Valenti, J. A. 2000, ApJ, 539, 815
Johns-Krull, C. M., & Valenti, J. A. 2001, ApJ, 561, 1060
Kaas, A. A. 1999, ApJ, 118, 558
Kelly, D. M., Rieke, G. H., & Campbell, B. 1994, ApJ, 425, 231
Kenyon, S. J., & Hartmann, L. 1995, ApJS, 101, 117
Hamann, F., DePoy, D. L., Johansson, S., & Elias, J. 1994, ApJ, 422, 626
Hartmann, L., Calvet, N., Avrett, E. H., & Loeser, R. 1990, ApJ, 349, 168
Hartmann, l., Calvet, N., Gullbring, E., & D'Alessio, P. 1998, ApJ, 495, 385
Hartigan, P., & Graham, J. A. 1987, AJ, 93, 913
Horrobin, M. J., Casali, M. M., & Eiroa, C. 1997, A&A, 320, L41
Lada, C. J., & Adams, F. C. 1992, ApJ, 393, 278
Luhman, K. L., & Rieke, G. H. 1998, ApJ, 497, 354
Marraco, H. G., & Rydgren, A. E. 1981, AJ, 86, 62
Meyer, M. R., Edwards, S., Hinkle, K. H., & Strom, S. E. 1998, ApJ, 508, 1998
Molinari, S., Liseau, R., & Lorenzetti, D. 1993, A&AS, 101, 59
Muzerolle, J., Hartmann, L., & Calvet, N. 1998, ApJ, 116, 2965
Najita, J., Carr, J. S., & Tokunaga, A. T. 1996, ApJ, 462, 919
Natta, A., Testi, L., Muzerolle, J., et al. 2004, A&A, 424, 603
Nisini, B., Antoniucci, S., & Giannini, T. 2004, A&A, 421, 187
Nisini, B., Caratti o Garatti, A., Giannini, T., & Lorenzetti, D. 2002, A&A, 393, 1035
Nisini, B., Smith, H. A., Fischer, J., & Geballe, T. R. 1994, A&A, 290, 463
Pontoppidan, K. M., Fraser, H. J., Dartois, E., et al. 2003, A&A, 408, 981
Rieke, G. H., & Lebofsky, M. J. 1985, ApJ, 288, 618
Siess, L., Forestini, M., & Bertout, C. 1997, A&A, 326, 1001
Siess, L., Forestini, M., & Bertout, C. 1999, A&A, 342, 480
Siess, L., Dufour, E., & Forestini, M. 2000, A&A, 358, 593
Taylor, K. N. R., & Storey, J. W. V. 1984, MNRAS, 209, 5P
Wallace, L., & Hinkle, K. 1996, ApJS, 107, 312
Wallace, L., & Hinkle, K. 1997, ApJS, 111, 445
Whitney, B. A., Wood, K., Bjorkman, J. E., & Cohen, M. 2003, ApJ, 598, 1079
Wilking, B. A., Taylor, K. N. R., & Storey, J. W. V. 1986, AJ, 92, 103
Wilking, B. A., Greene, T. P., Lada, C. J., Meyer, M. R., & Young, E. T. 1992, ApJ, 397, 520
Wilking, B. A., McCaughrean, M. J., Burton, M. G., et al. 1997, AJ, 114, 2029
Whittet, D. C. B., Smith, R. G., Adamson, A. J., et al. 1996, ApJ, 458, 363
Walmsely, C. M., Natta, A., Oliva, E., & Testi, L. 2000, A&A, 364, 301

Online Material

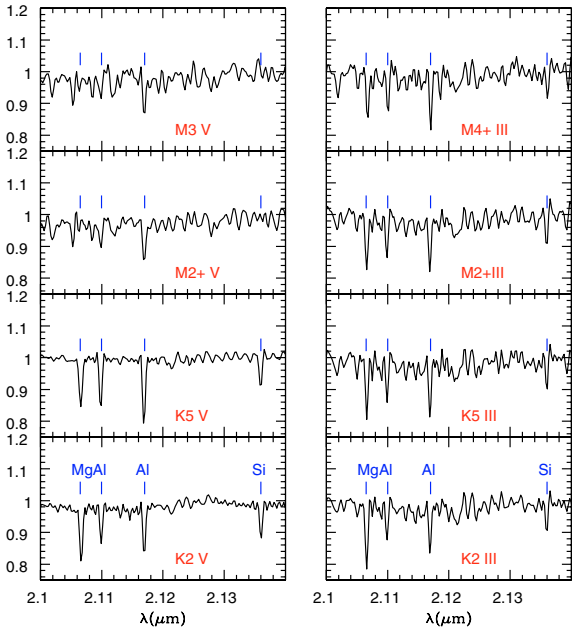

Fig. A.1. Spectra of dwarfs (*on the left*) and giant (*on the right*) standard stars taken from Wallace & Hinkle (1997) in a spectral segment around 2.1 μm, which includes spectral features of Mg, Al and Si.

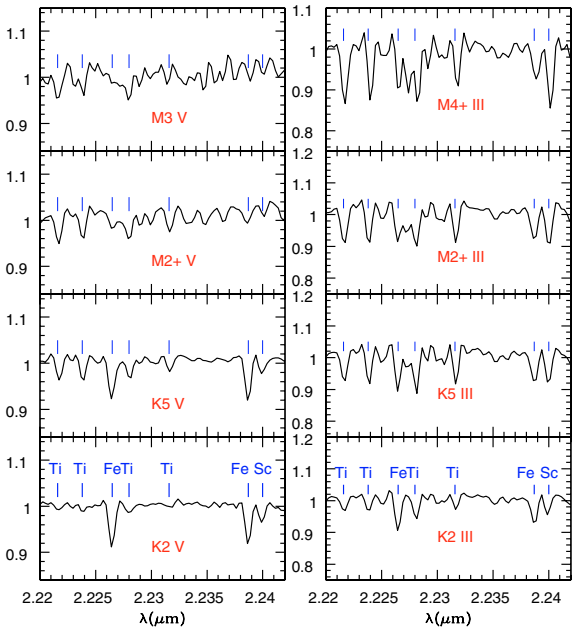

Fig. A.2. Spectra of dwarf (*on the left*) and giant (*on the right*) standard stars taken from Wallace & Hinkle (1997) in a spectral segment around 2.3 μm, which includes spectral features of Ti, Fe and Sc.

Appendix A: IR features selected for spectral classification

In the observed region of the *K* band we have identified two spectral segments, around 2.12 and 2.23 μm, where several features can be adopted for spectral classification. This can be seen in Figs. A.1 and A.2, where standard spectra are plotted of K and M spectral types, taken from the Wallace & Hinkle (1997) catalogue. In the spectra of dwarfs around 2.12 μm, Si at 2.1360 μm and Mg at 2.1066 μm weaken if one goes from early K to M types and hence their ratios with respect to the Al lines (2.1099, 2.1169 μm), whose EWs remain fairly constant, are sensitive to the effective temperature.

However, in the spectra of giants such ratios are less sensitive to the effective temperature, and therefore a K5V star can be easily confused with an M2III star. In order to distinguish also the spectral class, we can use other lines around 2.23 μm. For example the ratios Ti(2.2217, 2.2240 μm)/Fe(2.2266 μm) and Sc(2.2401 μm)/Fe(2.2386 μm) are significantly different for dwarfs and giants in K stars (Fig. A.2).

For the determination of the spectral type and luminosity class in our source sample we mainly adopted the above EW ratios in the *K* band, and checked a posteriori that the other observed features were well reproduced. The use of the features observed in the medium resolution *H* band spectral segment for the spectral type determination is limited due to the strong blending affecting most of the lines, and owing to the fact that the strongest and least blended lines, like Fe I at 1.637 μm and Si I at 1.639 μm, are not very sensitive to the effective temperature. On the other hand, this fact makes them very useful for determining the value of the veiling in the *H* band once the spectral type of the source has been derived from the analysis of the *K* band features.